Evolution of aerial spider webs coincided with repeated structural optimization of silk anchorages

Evolution of aerial spider webs coincided with repeated structural optimization of silk anchorages

Jonas O. Wolff[1*], Gustavo B. Paterno[1,2], Daniele Liprandi[3], Martín J. Ramírez[4], Federico Bosia[3], Arie van der Meijden[5], Peter Michalik[6], Helen M. Smith[7], Braxton Jones[1], Alexandra M. Ravelo[2], Nicola Pugno[8,9,10], and Marie E. Herberstein[1]

[1] Department of Biological Sciences, Macquarie University, Sydney, NSW 2109, Australia

[2] Instituto de Ciências Biológicas, Programa de Pós-Graduação em Ecologia, Universidade Federal de Juiz de Fora, Rua José Lourenço Kelmer, 36036-900, Juiz de Fora, MG, Brazil.

[3] Department of Physics and Nanostructured Interfaces and Surfaces Interdepartmental Centre, Università di Torino, Via P. Giuria 1, 10125 Torino, Italy

[4] Museo Argentino de Ciencias Naturales "Bernardino Rivadavia", Consejo Nacional de Investigaciones Científicas y Técnicas (CONICET), Av. Ángel Gallardo 470, C1405DJR, Buenos Aires, Argentina

[5] CIBIO Research Centre in Biodiversity and Genetic Resources, InBIO, Universidade do Porto, Campus Agrário de Vairão, Rua Padre Armando Quintas, 4485-661 Vairão, Vila do Conde, Portugal

[6] Zoologisches Institut und Museum, Universität Greifswald, Loitzer Str. 26, 17489, Greifswald, Germany

[7] Australian Museum, 1 William St, Sydney, New South Wales, 2010, Australia

[8] Laboratory of Bio-Inspired and Graphene Nanomechanics, Department of Civil, Environmental and Mechanical Engineering, University of Trento, Via Masiano 77, I-38123 Trento, Italy

[9] School of Engineering and Materials Science, Queen Mary University, Mile End Rd, London E1 4NS, UK

[10] KET Labs, Edoardo Amaldi Foundation, Italian Space Agency, Via del Politecnico snc, 00133 Rome, Italy

* corresponding author: jonas.wolff@mq.edu.au

Abstract

Physical structures built by animals challenge our understanding of biological processes and inspire the development of smart materials and green architecture. It is thus indispensable to understand the drivers, constraints and dynamics that lead to the emergence and modification of building behaviour. Here, we demonstrate that spider web diversification repeatedly followed strikingly similar evolutionary trajectories, guided by physical constraints. We found that the evolution of suspended webs that intercept flying prey was preceded by small changes in silk anchoring behaviour with considerable effects on the robustness of web attachment. The use of nanofiber based capture threads conflicts with the behavioural enhancement of web attachment, and the repeated loss of this trait has driven the evolution of web anchor structure. These findings show that the evolution of building behaviour may be constrained by major physical traits limiting its role in rapid adaptation to a changing environment.

Keywords

animal architecture; macro-evolution; evolutionary biomechanics; extended phenotype; spider silk; bio-inspiration

From efficient tunnel networks of ant colonies and strikingly effective thermal control of termite mounds to the aesthetic assembly of bower bird displays and ecosystem-forming beaver dams: the complexity, efficiency and far reaching effects of animal buildings excite and inspire [1] - their study may even drive technical innovation towards a greener future [2]. Our understanding of how building behaviour evolves within an ecological context is limited because animal architectures blur the boundaries of an organism's phenotype [3-5].

Spider webs are flagship examples of animal architectures, and their enormous diversity in shape render them an ideal system in which to unravel the evolutionary dynamics of building behaviour. Hypotheses of spider web evolution have been formulated for more than a hundred years, with a focus on the role of putatively singular events, such as the emergence of distinct building routines, specific silk proteins or viscid silk [6-10]. In contrast, recent[11-13] and controversial [14,15] phylogenomic studies favour a more dynamic scenario, where similar behavioural routines have repeatedly evolved. The core of the controversy is the question whether the evolution of behavioural building routines is dynamic and repeatable or slow and determined by contingent events. The answer to this question goes beyond spider webs: if the evolution of behaviour is less constrained than the evolution of physiological and morphological traits it could facilitate rapid responses to environmental changes, thereby setting the course of evolutionary trajectories [4,16,17].

Here, we approach the inference of spider web evolution from a previously neglected angle: the idea that a robust foundation is the basis for a stable building [1]. It has been proposed that the evolution of tape-like thread anchorages at the base of modern spiders (Araneomorphae) ~300 MYA dramatically changed silk usage: spiders were no longer restricted to spinning substrate-bound sheets, but could produce complex three dimensional structures by spatially arranging single lines [9,18]. Despite this early insight, subsequent work has focussed on the role web geometry and silk proteins in the evolution of webs, neglecting the role of web anchorages.

Since anchor strength underlies global mechanical rules, it is possible to derive parameter estimates for its optimization [19]. We hypothesized that lineages that achieve optimal anchor strength by behavioural means, also achieve web types with greater mechanical integrity. To test this, we quantified silk anchor structure and web types in 105 spider species of 45 families, covering all major clades of the modern spiders. We first built a numerical model to identify the optimum in anchor structure and tested if it matched the adaptive peaks in the macro-evolutionary signal. We then related silk anchor performance to anchor building behaviour and the morphology of the spinning apparatus. Specifically, we tested how the innate

spinneret choreography during anchor production affects anchor structure [18], and how the configuration of the spinning apparatus affects the kinematic properties of the system. Finally, we determined the sequence of silk anchor enhancement and aerial web evolution: did aerial web building lead to anchor enhancement, or were enhanced anchors a prerequisite for the evolution of aerial webs?

Results

Physical constraints and optima of silk anchorages

Web anchors resemble microscopic webs, consisting of numerous sub-micron sized glue coated fibres, so-called *piriform silk*. These fibres are combined into a patch-like film, taping the main thread, the *dragline*, onto the substrate. The dragline can be embedded all the way through this film, or be attached centrally only. The attachment position of the dragline greatly affects where and how load is transmitted onto the underlying film. The more central the dragline placement the better the anchor can withstand stress from a variably loaded silk line. Preliminary studies have revealed that this is the most significant determinant of web anchor robustness [20].

To identify the optimum of the dragline placement parameter c_d (dragline centrality), we built a numerical model based on the theory of thin film contact mechanics [21], approximating silk anchorages as tape like films. To apply our results to a range of silk properties found in spiders, we repeated simulations for parameters measured in the Tasmanian cave spider (*Hickmania troglodytes*), representing an ancient lineage, and in golden orb web spiders (*Nephila plumipes*), a representative of derived aerial web builders. We found that anchor strength improved if its geometrical structure allowed to maximize the peeling line (total length of the detachment front) before detachment, which occurred in the range c_d = 0.3–0.5 mm/mm for typical anchorage parameters (Fig. 1a). The exact optimum within this range depends, amongst others, on the material properties of the silk. For draglines as stiff as the anchor silk (or point-like dragline joints) c_d = 0.5 and it decreased with an increase in stiffness difference between dragline and anchor silk. During detachment, the stress concentrations and subsequent delamination front approximated a circular shape that became more elliptical as the peeling angle increased (Fig. 2b). The c_d value determined a delay in the detachment front reaching the anchorage edges (for typical anchorage shapes), leading to an overall increase in robustness. This is in agreement with empirical data on silk anchors of orb web spiders (S2) and up-scaled physical models [20]. Notably, the effect of the pulling angle on anchor resistance was reduced at

optimal c_d (Fig. 2c,d). This indicates that the benefit of high c_d is realised in dynamic loading situation, such as in aerial webs.

Evolutionary dynamics of spider web traits

Spider webs are diverse in shape and function but for the purpose of our analyses we categorised the web phenotypes into: 'substrate webs', 'aerial webs' and 'webless foragers' (see methods for definition). This reflects a different demand in mechanical stability and ecological impact of the web. Our phylogenetic analyses confirmed that substrate webs are the ancestral state in Araneomorphae. Aerial webs have evolved independently at the basis of Araneoidea, in Uloboridae, Deinopidae, Pholcidae, and within Desidae.

Lineages with anchors near the physical optimum of c_d = 0.3–0.5 included all aerial web builders that lack a cribellum, the cribellate substrate web building Megadictynidae, and some ecribellate hunting spiders of the Mimetidae, Arkyidae, Thomisidae, Oxyopidae, Trechaleidae, Philodromidae, Salticidae and Toxopidae. We found multiple support for six shifts in the evolutionary regime of c_d : *shift 1* in Pholcidae (posterior probability *pp* = 0.494); *shift 2* in the grate-shaped tapetum clade (excl. Zoropsidae) (*pp* = 0.474); *shift 3* at the basis of Salticidae (*pp* = 0.405); *shift 4* at the basis of Entelegynae (*pp* = 370); *shift 5* at the basis of Araneoidea (*pp* = 0.336); and *shift 6* within Desidae (*Cambridgea*) (*pp* = 0.309). Shift 5 and 6 (both aerial web spinners; adaptive optimum $\theta \sim 0.36$ mm/mm), and shifts 1, 2 and 3 (aerial web spinning and hunting spiders; $\theta \sim 0.30$ mm/mm) were convergent, shifting towards similar evolutionary optima (Fig. 3f). Shifts 2, 5 and 6 coincided with cribellum loss and shifts 1 and 5 with the evolution of aerial webs. Notably all supported shifts led towards an elevated adaptive optimum θ. Our data suggest that the evolutionary trend towards an elevated c_d happened stepwise, for instance the exceptional c_d in Araneoidea evolved from an estimated root optimum of $\theta \sim 0.18$ mm/mm, with the first shift around 250 MYA towards $\theta \sim 0.24$ mm/mm (shift 4), and the second one around 180 MYA towards $\theta \sim 0.36$ mm/mm (shift 5). The exact location of these shifts differed between *SURFACE* and *bayou* methods, and an additional shift at the basis of Nicodamidoidea+Araneoidea around 200 MYA is possible (*pp* = 0.290; Fig. 2; S4; S5). In Uloboridae and Deinopidae only one step occurred (shift 4), approximately 50 MY prior to aerial web evolution in these families. In Pholcidae the single regime shift (shift 1) coincided with aerial web evolution.

We found evidence that the evolution of high c_d values has been constrained by the configuration of the spinning apparatus. Spiders with a spinning plate - the cribellum (the basal state) produced a significantly smaller c_d (p = 0.009; S6) and cribellum loss generally led to an

increase of c_d (Fig. 3b). Furthermore, c_d correlated with spinning choreography, i.e. the relative height of the spinneret trajectory geometry h_r (p = 0.004; S6): h_r is on average 1.6 times larger in ecribellate spiders (p < 0.001; S6). These results were highly robust to phylogenetic uncertainty (S6). Notably, the shape of the spinning path did not differ between cribellar and ecribellar spiders (p_r = 0.214) (S7). This indicates that it is not the shape of the spinning path, but its orientation and proportions that affect c_d. Our kinematic and morphological studies revealed that the cribellum mechanically constrains the mobility of the anchor producing spinnerets (the anterior lateral spinnerets) by blocking them on the anterior side. As a result, most cribellar spiders spread the spinnerets more laterally, leading to smaller h_r and c_d.

To further investigate if the configuration of the spinning apparatus (c) and web building behaviour (w) had an effect on the evolutionary dynamics of c_d, we compared the fit of single and two-regime Brownian Motion (BM) and Ornstein-Uhlenbeck (OU) models. To account for phylogenetic uncertainty, we repeated the analyses across a sample of 100 phylogenetic trees.

We found strong support for a scenario, where the evolution of anchor structure was highly dynamic in substrate web builders and hunters, but stabilized around an elevated optimum in aerial web builders. Among all models, OUw models provided the best explanation for the extant variation of c_d (*AICcw* (OUMVAw) = 0.667±0.339; *AICcw* (OUMAw) = 0.163±0.295; Fig. 3a). Under these models c_d evolved at an increased adaptive optimum with a high adaptive potential in aerial web builders, while c_d of substrate web building and hunting spiders followed a stochastic evolution (i.e. $t½ >> T$; Fig. 3b,c). There was support that cribellum loss affected the evolution of c_d (mean $\Delta AICc$ (OUMc-BM1) = 3.43, mean $\Delta AICc$ (OUMc-OU1) = 4.34). The best fit among OUc-models was the OUMc, a model under which c_d of ecribellar spiders had a higher adaptive optimum θ but evolutionary rates σ^2 and adaptive potential α did not differ between cribellar and ecribellar spiders. The inferred mean $t½$ was close to the total height of the tree T, which represents a moderate α [22].

Similar analyses on the spinning track proportions h_r indicated five shifts in the evolutionary regime: *shift 1* within Desidae (*Cambridgea*) (*pp* = 0.507); *shift 2* at the basis of Hersiliidae (*pp* = 0.584); *shift 3* at the basis of Araneoidea (*pp* = 0.579); *shift 4* in the grate-shaped tapetum clade (excl. Zoropsidae) (*pp* = 0.590); and shift 5 in Pholcidae (*pp* = 0.470) (Fig. 2). All but shift 5 coincided with cribellum loss, and shifts 1, 3 and 5 co-occurred with aerial webs. Branches accommodating shifts 1, 3, 4 and 5 also had shifts in c_d, indicating a causal link. The constitution of the spinning apparatus had clearly affected the evolution of h_r (*AICcw*(OUMAc) = 0.442 ±0.247; *AICcw*(OUMVAc) = 0.388 ±0.269), whereas OUw models were indistinguishable from BM models (Fig. 3d). The contrasting results for c_d indicate that h_r

alone does not explain c_d. There is, at least, one additional behavioural component affecting c_d, which is the movement of the body while a series of alternating spinneret movements are performed. The highest c_d values (excluding the hunting spider *Australomisidia*) were found in spiders that perform a back-and-forth movement of the abdomen during anchor production. This behaviour has evolved independently in the Araneoidea and in *Cambridgea*.

Discussion

This study is the first to assess attachment as a driving component in the evolution of animal architectures. We have shown that small changes in anchor structure profoundly affect web attachment. Notably, structural optimization does not necessarily come at a higher material cost, as the effect of dragline placement is significant for similar sized silk films. It therefore appears counter-intuitive that not all extant spiders exhibit an optimized anchor structure and that anchor building behaviour evolved slowly and stepwise. We found this is due to two reasons: first, the evolution of anchor structure is relaxed in substrate web builders and wandering spiders that do not rely on robust silk anchorages, and second, the evolution of anchor building behaviour is constrained by physical traits.

Our data suggests that the cribellum organ, a sophisticated spinning plate that produces nanofiber-based capture threads, is one example of such a physical constraint on behavioural evolution. This is important since it provides an explanation for an old enigmatic problem in the understanding of spider web evolution: why nano-fibre capture silk was lost so frequently across the spider tree, resulting in cribellar spiders being largely outnumbered by ecribellar spiders, and why only few cribellar spiders evolved aerial webs, even though cribellar silk can be highly efficient in prey capture [23-25]. Our results indicate that the cribellum represents a significant constraint on the evolution of robust anchorages limiting the capability to build efficient suspended webs.

We found that all changes in the evolutionary mode of anchor spinning behaviour followed or co-occurred with the loss of the cribellum. However, cribellum loss did not lead to changes in the evolutionary dynamics of spinning behaviour *per se*, indicating that further changes of physical traits, such as the arrangement of muscles and spinneret articulation, might have been necessary to alter spinning behaviour in a way to optimize anchor structure. Cribellum loss was thus an important pre-condition for further evolutionary enhancement of silk attachment.

Multiple support for an exceptional (i.e. faster and more stabilized) evolution of anchor structure in aerial web builders underlines its adaptive value for such webs. Aerial webs repeatedly evolved after evolutionary shifts in silk anchor structure and anchor spinning behaviour occurred supporting the idea that web anchor performance mediates the evolution of web architecture.

Limited anchor performance may thus in itself be an important constraint in the evolution of web building behaviour, and its improvement may have accelerated spider web diversification: web architecture is phylogenetically labile and enormously variable in ecribellate orb-web and cobweb spiders [26-28], lineages in which anchor structure has reached the physical optimum. Such a rapid turnover of web building behaviour may mask evolutionary histories in these lineages. Concluding that similarities in building routines indicate a common origin can be problematic in these cases, since the probability of parallelism is high [16,29]. Our example shows that to understand the evolution of complex behaviour, like orb-web building, it is essential to identify the interdependencies of behavioural and physical traits.

We conclude that the evolution of behaviour and extended phenotypes is not as free as previously suggested [4,30-32], but may be tightly bound to evolutionary changes in physical traits. In the case of spider webs the evolutionary removal of such constraints has led to an evolutionary cascade resulting in an enormous diversity of web architectures and outstanding ecological success.

Material and Methods

Material sourcing and fieldwork

Spiders were collected in Eastern Australia (NSW, QLD, VIC and TAS), New Zealand (North Island), Germany, Italy, the U.S.A., Argentina and Morocco, or obtained from lab stocks (3 species) and kept in the lab in plastic jars or boxes with slightly moistened tissue (complete list of species and collection data in Tab. S8). We aimed for three individuals per species, while we did not expect differences in our target traits between sexes and developmental stages (confirmed by intraspecific comparison of anchor structure in *Argiope keyserlingi* and *Nephila plumipes*, unpub.). However, for some species only single individuals could be obtained (samples sizes are given in Tab. S1 and Fig. 2). Silk samples were collected on glass slides that were left in the enclosures for 2-7 days. Silk samples were stored in dry boxes and are deposited at the Department of Biological Sciences, Macquarie University (MQ). Voucher specimens of spiders are deposited at the Australian Museum (AM), the Zoological Museum of the University of Greifswald (UG), the Natural History Museum of Argentina (MA), Canterbury Museum (CM) and private collections (see Tab. S8 for details).

For each species we recorded the web type based on field and lab observations: 0, no web (hunting spider); 1, substrate bound web (capture area ± parallel and directly attached to the substrate surface); 2, aerial web (capture

area suspended, indirectly attached to substrate, and its shape ± independent of substrate topography). These categories were chosen, because they represent different demands of a robust anchorage.

Morphology of spinning apparatus

Spiders were investigated under dissection microscopes to score two states of the spinning apparatus: 0, ecribellar; 1, cribellar.

Kinematics of spinning apparatus

Spinning choreography was studied in a subset of 71 species following the methods described in [20], using a Basler Ace 640×480pix USB 3.0 high speed video camera (Basler AG, Ahrensburg, Germany), equipped with a Navitar Precise Eye extension tube including a 1.33× magnification lens (Navitar, Inc., Rochester, NY, USA). A 0.25× accessory lens was used for larger spiders (body length >10 mm). The resulting field of view was 1.3 × 1.0 mm at a pixel size of 2.1 µm for the basic configuration, and 5.3 × 4.0 mm at a pixel size of 8.3 µm for the configuration with the 0.25× lens. Videos were recorded with 500 frames per second, using the *TroublePix* software (NorPix, Inc., Montreal, QC, Canada) with continuous looping and post event trigger.

Videos were processed with *ImageJ 1.5* [33] as detailed in [20]. The movements of both anterior lateral spinnerets were manually tracked using the *MTrackJ* plugin [34], taking the centre of the piriform spigot field on the anterior lateral spinneret apex as a reference. Each spinning sequence consists of a set of stereotypic spinneret trajectories. Single trajectories were extracted, their tracking coordinates positioned in a generalized grid and partitioned into 50 landmarks defined by regularly spaced time intervals (for details on this procedure we refer to [18,20]). This procedure ensures that the relative orientation of the kinematic track shapes towards the animal's body axis is maintained. From these shapes we calculated the relative track proportions h_r as the *y*-dimension divided by the *x*-dimension of the aligned track shape, where the minimal *x*-coordinate denotes the proximal turning point of the adducted spinneret (where the dragline is usually placed) and the maximal *x*-coordinate the lateral turning point of the abducted spinneret. This variable reflects under which angle piriform silk is spread away from the dragline joint.

The final dragline location may not only be determined by the trajectories of single kinematic elements, but also how these are applied along the animal's body axis. Some spiders perform a back-and-forth movement of the abdomen to further modulate dragline placement. This behaviour was recorded as a binary character: 0, absent; 1, present.

Structure and morphometrics of silk anchors

Nine to twenty silk anchors per individual spider were imaged with Leica M205A (Leica Microsystems GmbH, Wetzlar, Germany) and Motic (Motic Inc. Ltd., Hong Kong) stereo microscopes with mounted cameras.

Morphometrics of silk anchors was performed on micrographs in *ImageJ*. We calculated the dragline placement variable c_d as follows: distance *d* between the dragline joint (point were the dragline leaves the anchor) and the anterior border of the anchor divided by the longitudinal dimension of the anchor. In anchors of some basal species the individual dragline fibres do not leave the anchor as a bundle, but separately in different locations. In these cases the pair of fibres located closest to the frontal border of the anchor was taken into consideration and their *d*-values were averaged. Details on the morphometric characterization of silk anchors are described in [20].

Numerical model

The elastic membrane was modelled by discretising it in a network of elastic bonds (i.e. springs) in a square-diagonal lattice, using a generalized non-linear 3D co-rotational truss formulation [35]. A homogenization procedure was adopted, imposing the equivalence of the strain energy density of the lattice with that of a corresponding homogeneous membrane [36,37]. We used a standardized anchor geometry with length l = 1 mm, width w = 1 mm, thickness t = 1 μm, and with the dragline fused with the membrane over a length of c_l = 0.33 mm. To account for differences in silk properties, we performed separate simulations for a combination of membrane and dragline stiffness values, as empirically observed in the basal sheet web spider *H. troglodytes* and the aerial web builder *N. plumipes*: Young's modulus of piriform silk membrane E_p = 0.25 GPa for *Hickmania* and E_p = 1.7 GPa for *Nephila* (see tensile test methodologies and results in S1), and Young's modulus of dragline E_d = 10 GPa for *Hickmania* and E_d = 15 GPa for *Nephila* (after [38] and [39]).

The interface was modelled assuming a 3D exponential-like traction-separation law (cohesive zone model) of the form $T_i = \Delta_i \frac{\phi_i}{\delta_i^2} \cdot \exp\left(\sum_j - \frac{\Delta_j^2}{\delta_j^2}\right)$ where ϕ_i, Δ_i and δ_i are the work of separation, the crack gap value and the characteristic length (i.e. the gap value corresponding to the maximum traction) [40]. The resulting system of coupled non-linear equations in matrix form was solved using an algorithm based on the Newton-Raphson method [41] implemented in C++ and run on the OCCAM HPC cluster at the University of Torino. The adhesive energy of the interface, calculated as the integral of the cohesive law, was taken to be equal to ϕ = 0.5 MPa·mm.

We simulated the maximal pull-off forces for different c_d between 0.0 and 0.5. To further study the effect of c_d on anchor robustness we simulated maximal pull-off forces for different pull-off angles (loading angles) between 15° (± parallel to substrate along spinning direction) and 165° (± parallel to substrate against spinning direction, e.g. dragline flipped over) for a c_d of 0.0, 0.2 and 0.4.

Phylogenetic inference

The phylogenetic tree was estimated using three mitochondrial (12S, 16S, COI) and three nuclear (histone H3, 18S, 28S) markers, taken from the study of Wheeler et al. [42] and supplemented with sequences from GenBank (Table S10). The clades obtained as monophyletic in the genomic analyses of Fernández et al. [11] (Araneae), Kallal et al. [43] (Araneidae), Cheng and Piel [44] (oval calamistrum clade), and Maddison et al. [45] (Salticidae) were constrained for monophyly, as a backbone tree. The reason for such constrained analysis is that our six-markers dataset will not have sufficient signal to overturn the results based on hundreds to thousands of markers from the genomic analyses.

We lacked sequence data for 58 of the studied species but were able to use sequences from closely related species to obtain a good estimate of phylogenetic placement and branch lengths (Table S9). For an additional set of 20 species we did not have close relatives, or a close relative was already in the dataset; these were connected randomly in internal branches according to their taxonomic placement (Table S9). Two non-araneomorph terminals were added to root the tree, representing the lineages Mesothelae and Mygalomorphae; these were excluded from the comparative analyses.

Alignment of sequences was performed with *MAFFT* version 7 online service [46]. Model selection was made with *jModeltest* [47]. Secondary dating of main tree nodes was assigned as mean and 95% HPD taken from Fernández et al. [11] and analysed in *BEAST2* [48] under a relaxed lognormal clock model [49], using the CIPRES Science Gateway [50] for 50 million generations. After a pilot run, GTR models were simplified to HYK to achieve

convergence. The 20 species without sequence data were free to connect anywhere along any branch within taxonomically constrained clades; to avoid for very short tip branches, we placed a uniform prior for the clade age, with minimum 2 mya for congeners and 5 mya for higher taxa.

To account for the uncertainty of the phylogenetic estimation, we obtained 100 trees randomly drawn from the post-burnin posterior sample of the Bayesian analysis in *BEAST2*. The subsequent comparative analyses are averaged over these 100 trees, and thus incorporate the uncertainty in phylogenetic parameters.

Macro-evolutionary framework

We used phylogenetic comparative methods to infer adaptive peaks and constraints and test evolutionary associations of silk anchor structure, spinning apparatus, spinning kinematics and web building behaviour, using multiple packages in the software environment *R*.

Ancestral state estimation of spinning apparatus morphology was performed with stochastic character mapping using the *make.simmap* function in *phytools* [51], with 100 repeats using Equal Rates (*ER*), All Rates Different (*ARD*) and customized models. State 1 (cribellum present) was returned in the ancestral node in all cases, but there were two cases of cribellum loss and re-gain under the ER and ARD models. Since this is a highly unlikely scenario (see [52]), we introduced a rate substitution matrix that supressed state 1 to 2 transitions. The returned simmaps were used to locate events of cribellum loss and for *OUwie* analyses. Ancestral state estimation of web type was done with *ace* in *ape* 5.1 [53] using ER and ARD models.

To infer evolutionary dynamics of the continuous variables dragline placement c_d and spinning track dimensions h_r we used a multi-step model-selection process. To test if changes in discreet characters led to differential evolutionary dynamics, we fitted different Brownian Motion (*BM*) and generalized Ornstein-Uhlenbeck-based Hansen models (*OU*) using the package *OUwie* 1.50 [54]. We built a set of models for spinning apparatus state (*c*) and web type (*w*, web type was binary discretized for this purpose in aerial web: 0, no; 1, yes) using a randomly drawn simmap of *c*- and *w*-regimes for each of the 100 trees from our sample. We tested a single-regime BM (*BM1*) and OU model (*OU1*), and per regime type each a two-σ^2 (*BMS*) BM model, and OU models with two θ (*OUM*), two θ and two σ^2 (*OUMV*), two θ and two α (*OUMA*), and two θ, two σ^2 and two σ^2 (*OUMVA*). The corrected Akaike information criterion (*AICc*) was used to compare the fit between all 12 models by calculating the *AICc* weight (*AICcw*) for each tree. *AICcw* and model parameters were then summarized across all 100 trees and their median and variance assessed to select for the model(s) that could best explain the data. For each c_d and h_r we ran two loops across the tree sample to check for the effect of the stochastic component in this procedure, and found comparable results (i.e. similar models were favoured and no major differences in median parameter estimates).

While prior clade assignments are useful to compare defined groups, they may miss some hidden patterns caused by unstudied effects. We therefore additionally used the methods *SURFACE* [55] and *bayou* [56] on the consensus tree (S3). *SURFACE* performs stepwise AIC estimation to identify regime shifts in θ assuming evolution under the OU process with constant σ^2 and α. *bayou* uses a reverse-jump Markov chain Monte Carlo procedure for the similar purpose. By this, we also checked, if evolution of our variables was driven by singular events (i.e. the occurrence of only a single shift), which may bias PGLS inference [57]. Because the results of *bayou* can be sensitive to the mean number of shifts in the prior [56,58], we ran each two chains over 500,000 generations for prior means of 10, 15, 20, and 25 shifts with equal shift probability and one shift maximum per branch, discarding the first 30% as burn-in. For c_d chains with priors of 20 and 25 shifts and for h_r chains with priors of 15, 20 and 25 shifts arrived

at a similar posterior (S5). Results are reported from these chains only (means of converged chains given, and graphical representation of shifts for c_d from a randomly chosen chain with a prior of 25 shifts and for h_r from a randomly chosen chain with a prior of 20 shifts).

Trait correlation

To reveal patterns of trait correlation we used phylogenetic generalized least squares models (PGLS), which accounts for the non-independence of observations due to common evolutionary history [59-61], across pairwise combinations of our variables: (1) c_d ~ *spinning apparatus*; (2) c_d ~ *web type*; (3) h_r ~ *spinning apparatus*; and (4) h_r ~ *web type*. Further, we performed PGLS regressions between c_d ~ h_r. PGLS analyses were performed with the R package *phylolm* [62] and branch length transformation were optimized by setting *lambda* value through maximum likelihood. To account for phylogenetic uncertainty in PGLS results [63] we repeated each model across our posterior sample of 100 phylogenetic trees. The influence of phylogenetic uncertainty on results was estimated by the variation in model parameters across all runs. Phylogenetic sensitivity analyses were performed for each PGLS model with the R package *sensiPhy* [64].

Geometric Morphometrics

To test if the shape of spinning paths differed between spiders with different spinning apparatus and web type, and if it correlates with c_d and h_r, geometric morphometrics was performed using the R package *geomorph* [65]. For this purpose aligned spinneret trajectories were discretized into 50 landmarks with similar time steps, as described in [18]. We used both an alignment towards the median axis between the paired spinnerets which keeps the angular orientation of the trajectories (see [18]), and General Procrustes Alignment (GPA), which omits this information and extracts the pure shape. We then performed Phylogenetic Procrustes ANOVA against the variable 'spinning apparatus' and 'web type' and Phylogenetic Procrustes Regression against variables c_d and h_r using the consensus tree.

Acknowledgements

We are grateful to the following people, who assisted in the filming of spinning behaviour, spider and silk sample collection, and spider maintenance, provided material and access to facilities, or helped with field trip logistics and spider identification: Mohammad Ameri, Arthur Clarke, Niall Doran, Jessica Garb, Arno Grabolle, Stanislav Gorb, Cristian Grismado, William Haynes, Siegfried Huber, Anna-Christin Joel, Alex Jordan, Lachlan Manning, Bryce McQuillan, Graham Milledge, Anna Namyatova, Nicole O'Donnell, John Osmani, Robert Raven, Birte Schadlowski, Cristina Scioscia, Wolfgang Schlegel, Axel Schönhofer, Angela Simpson, Gabriele Uhl, Cor Vink, Zoe Wild, and Lydia Wolff.

Some animals were collected under license SL101868 (Australia) and 64293-RES (New Zealand).

Funding

This study was supported by a Macquarie Research Fellowship of Macquarie University to JOW. FB was supported by the FET Proactive "Neurofibres" grant No. 732344, the COST Action CA15216 "European Network of Bioadhesion Expertise", and by Progetto d'Ateneo/Fondazione San Paolo "Metapp", n. CSTO160004. NMP was supported by the European Commission H2020 under the Graphene Flagship Core 2 No. 785219 (WP14

"Composites") and the FET Proactive "Neurofibres" grant No. 732344, as well as by the Italian Ministry of Education, University and Research (MIUR) under the "Departments of Excellence" grant L.232/2016. MR was supported by the Agencia Nacional de Promoción Científica y Tecnológica, Argentina grant PICT-2015-0283. AvdM was supported by a grant by FCT under the Programa Operacional Potencial Humano – Quadro de Referência Estratégico Nacional funds from the European Social Fund and Portuguese Ministério da Educação e Ciência (SFRH/BPD/101057/2014). Computational resources were provided by the Centro di Competenza sul Calcolo Scientifico (C3S) of the University of Torino (c3s.unito.it).

Author contributions

JOW devised, led and administered the project. JOW, BJ, AMR and PM collected the data. MJR performed the phylogenetic inference. GBP, JOW and AvdM performed the phylogenetic comparative analysis. NMP and FB developed and supervised, and DL carried out the physical numerical simulations. H.S. and M.J.R. ensured taxonomic integrity. JOW, FB and MEH wrote the manuscript. All authors critically revised the manuscript and approved its final version. M.E.H. and N.M.P. mentored the project.

Competing Interests

The authors declare that they have no conflict of interests.

Data accessibility

Data matrices, trees, R code and additional details of statistical results are deposited in the electronic supplemental material of this paper.

References

1 Hansell, M. H. *Animal architecture*. (Oxford University Press, 2005).
2 Turner, J. S. & Soar, R. C. in *First International Conference on Industrialized, Intelligent Construction at Loughborough University.* (eds I. Wallis, L. Bilan, M. Smith, & A. S. Kaz).
3 Dawkins, R. (Oxford: Oxford University Press, 1982).
4 Odling-Smee, F. J., Odling-Smee, H., Laland, K. N., Feldman, M. W. & Feldman, F. *Niche construction: the neglected process in evolution*. (Princeton university press, 2003).
5 Bailey, N. W. Evolutionary models of extended phenotypes. *Trends Ecol Evol* **27**, 561-569 (2012).
6 Eberhard, W. G. Function and phylogeny of spider webs. *Annual review of Ecology and Systematics* **21**, 341-372 (1990).
7 Blackledge, T. A. *et al.* Reconstructing web evolution and spider diversification in the molecular era. *Proceedings of the National Academy of Sciences* **106**, 5229-5234 (2009).
8 Bond, J. E. & Opell, B. D. Testing adaptive radiation and key innovation hypotheses in spiders. *Evolution* **52**, 403-414 (1998).
9 Coddington, J. A. in *Spiders of North America: an identification manual.* (eds D Ubick, P Paquin, P.E. Cushing, & V. Roth) 18-24 (American Arachnological Society, 2005).
10 Coddington, J. A. in *Spiders. Webs, Behavior, and Evolution* (ed W.A Shear) 319-363 (Stanford University Press, 1986).
11 Fernández, R. *et al.* Phylogenomics, diversification dynamics, and comparative transcriptomics across the spider tree of life. *Curr Biol* **28**, 1489-1497 (2018).
12 Bond, J. E. *et al.* Phylogenomics resolves a spider backbone phylogeny and rejects a prevailing paradigm for orb web evolution. *Curr Biol* **24**, 1765-1771 (2014).
13 Fernández, R., Hormiga, G. & Giribet, G. Phylogenomic analysis of spiders reveals nonmonophyly of orb weavers. *Curr Biol* **24**, 1772-1777 (2014).
14 Garrison, N. L. *et al.* Spider phylogenomics: untangling the Spider Tree of Life. *PeerJ* **4**, e1719 (2016).
15 Eberhard, W. G. Modular patterns in behavioural evolution: webs derived from orbs. *Behaviour* **155**, 531-566 (2018).

16 Ord, T. J. & Summers, T. C. Repeated evolution and the impact of evolutionary history on adaptation. *Bmc Evol Biol* **15**, 137 (2015).
17 Wcislo, W. T. Behavioral environments and evolutionary change. *Annual Review of Ecology and Systematics* **20**, 137-169 (1989).
18 Wolff, J. O., van der Meijden, A. & Herberstein, M. E. Distinct spinning patterns gain differentiated loading tolerance of silk thread anchorages in spiders with different ecology. *Proceedings of the Royal Society B: Biological Sciences* **284**, 20171124 (2017).
19 Pugno, N. M., Cranford, S. W. & Buehler, M. J. Synergetic material and structure optimization yields robust spider web anchorages. *Small* **9**, 2747-2756, doi:DOI 10.1002/smll.201201343 (2013).
20 Wolff, J. O. & Herberstein, M. E. 3D-printing spiders: back-and-forth glue application yields silk anchorages with high pull-off resistance under varying loading situations. *J R Soc Interface* **14**, 20160783 (2017).
21 Pugno, N. M. The theory of multiple peeling. *Int J Fracture* **171**, 185-193 (2011).
22 Cooper, N., Thomas, G. H., Venditti, C., Meade, A. & Freckleton, R. P. A cautionary note on the use of Ornstein Uhlenbeck models in macroevolutionary studies. *Biol J Linn Soc* **118**, 64–77 (2016).
23 Bott, R. A., Baumgartner, W., Bräunig, P., Menzel, F. & Joel, A.-C. Adhesion enhancement of cribellate capture threads by epicuticular waxes of the insect prey sheds new light on spider web evolution. *Proc. R. Soc. B* **284**, 20170363 (2017).
24 Opell, B. D. & Schwend, H. S. Adhesive efficiency of spider prey capture threads. *Zoology* **112**, 16-26 (2009).
25 Opell, B. The ability of spider cribellar prey capture thread to hold insects with different surface features. *Funct Ecol*, 145-150 (1994).
26 Blackledge, T. A. & Gillespie, R. G. Convergent evolution of behavior in an adaptive radiation of Hawaiian web-building spiders. *Proceedings of the National Academy of Sciences* **101**, 16228-16233 (2004).
27 Kuntner, M., Kralj-Fišer, S. & Gregorič, M. Ladder webs in orb-web spiders: ontogenetic and evolutionary patterns in Nephilidae. *Biol J Linn Soc* **99**, 849-866 (2010).
28 Eberhard, W. G., Agnarsson, I. & Levi, H. W. Web forms and the phylogeny of theridiid spiders (Araneae: Theridiidae): chaos from order. *Systematics and biodiversity* **6**, 415 (2008).
29 York, R. A. & Fernald, R. D. The Repeated Evolution of Behavior. *Frontiers in Ecology and Evolution* **4**, 143 (2017).
30 West-Eberhard, M. J. Phenotypic plasticity and the origins of diversity. *Annual review of Ecology and Systematics* **20**, 249-278 (1989).
31 Bailey, N. W., Marie-Orleach, L. & Moore, A. J. Indirect genetic effects in behavioral ecology: does behavior play a special role in evolution? *Behav Ecol* **29**, 1-11 (2018).
32 Duckworth, R. A. The role of behavior in evolution: a search for mechanism. *Evolutionary ecology* **23**, 513-531 (2009).
33 Schneider, C. A., Rasband, W. S. & Eliceiri, K. W. NIH Image to ImageJ: 25 years of image analysis. *Nat methods* **9**, 671-675 (2012).
34 Meijering, E., Dzyubachyk, O. & Smal, I. Methods for Cell and Particle Tracking. *Methods in Enzymology* **504**, 183-200 (2012).
35 Cook, R. D., Malkus, D. S. & Plesha, M. E. *Concepts and applications of finite element analysis*. (John Wiley & Sons, 2001).
36 Ostoja-Starzewski, M. Lattice models in micromechanics. *Applied Mechanics Reviews* **55**, 35-60 (2002).
37 Brely, L., Bosia, F. & Pugno, N. M. A hierarchical lattice spring model to simulate the mechanics of 2-D materials-based composites. *Frontiers in Materials* **2**, 51 (2015).
38 Piorkowski, D. *et al.* Ontogenetic shift toward stronger, tougher silk of a web-building, cave-dwelling spider. *J Zool* **304**, 81-89 (2018).
39 Swanson, B., Blackledge, T., Beltrán, J. & Hayashi, C. Variation in the material properties of spider dragline silk across species. *Applied Physics A* **82**, 213-218 (2006).
40 Salehani, M. K. & Irani, N. A coupled mixed-mode cohesive zone model: An extension to three-dimensional contact problems. *arXiv preprint arXiv:1801.03430* (2018).
41 Ostrowski, A. M. in *Third Edition of Solution of Equations and Systems of Equations* Vol. 9 *Pure and Applied Mathematics* (ed A.M. Ostrowski) 53-55 (Elsevier, 1973).
42 Wheeler, W. C. *et al.* The spider tree of life: phylogeny of Araneae based on target-gene analyses from an extensive taxon sampling. *Cladistics* **33**, 574-616 (2017).
43 Kallal, R. J., Fernández, R., Giribet, G. & Hormiga, G. A phylotranscriptomic backbone of the orb-weaving spider family Araneidae (Arachnida, Araneae) supported by multiple methodological approaches. *Mol Phylogenet Evol* **126**, 129-140 (2018).
44 Cheng, D.-Q. & Piel, W. H. The origins of the Psechridae: Web-building lycosoid spiders. *Mol Phylogenet Evol* **125**, 213-219 (2018).

45 Maddison, W. P. *et al.* A genome-wide phylogeny of jumping spiders (Araneae, Salticidae), using anchored hybrid enrichment. *Zookeys*, 89 (2017).

46 Katoh, K., Rozewicki, J. & Yamada, K. D. MAFFT online service: multiple sequence alignment, interactive sequence choice and visualization. *Briefings in bioinformatics* (2017).

47 Darriba, D., Taboada, G. L., Doallo, R. & Posada, D. jModelTest 2: more models, new heuristics and parallel computing. *Nature methods* **9**, 772 (2012).

48 Bouckaert, R. *et al.* BEAST 2: a software platform for Bayesian evolutionary analysis. *Plos Comput Biol* **10**, e1003537 (2014).

49 Drummond, A. J., Ho, S. Y., Phillips, M. J. & Rambaut, A. Relaxed phylogenetics and dating with confidence. *PLoS biology* **4**, e88 (2006).

50 Miller, M. A., Pfeiffer, W. & Schwartz, T. in *Gateway Computing Environments Workshop (GCE), 2010.* 1-8 (Ieee).

51 Revell, L. J. phytools: an R package for phylogenetic comparative biology (and other things). *Methods in Ecology and Evolution* **3**, 217-223 (2012).

52 Miller, J. A. *et al.* Phylogenetic affinities of the enigmatic spider family Penestomidae (new rank), generic phylogeny of Eresidae, and other advances in spider phylogeny (Araneae, Araneoidea, Entelegynae). *Mol Phylogenet Evol* **55**, 786–804 (2010).

53 Paradis, E., Claude, J. & Strimmer, K. APE: analyses of phylogenetics and evolution in R language. *Bioinformatics* **20**, 289-290 (2004).

54 Beaulieu, J. & O'Meara, B. OUwie: analysis of evolutionary rates in an OU framework. *R package version* **1** (2014).

55 Ingram, T. & Mahler, D. L. SURFACE: detecting convergent evolution from comparative data by fitting Ornstein-Uhlenbeck models with stepwise Akaike Information Criterion. *Methods in Ecology and Evolution* **4**, 416-425 (2013).

56 Uyeda, J. C. & Harmon, L. J. A novel Bayesian method for inferring and interpreting the dynamics of adaptive landscapes from phylogenetic comparative data. *Systematic biology* **63**, 902-918 (2014).

57 Uyeda, J. C., Zenil-Ferguson, R. & Pennell, M. W. Rethinking phylogenetic comparative methods. *Systematic Biology*, syy031 (2018).

58 Ho, L. S. T. & Ané, C. Intrinsic inference difficulties for trait evolution with Ornstein-Uhlenbeck models. *Methods in Ecology and Evolution* **5**, 1133-1146 (2014).

59 Felsenstein, J. Phylogenies and the comparative method. *The American Naturalist* **125**, 1-15 (1985).

60 Grafen, A. The phylogenetic regression. *Phil. Trans. R. Soc. Lond. B* **326**, 119-157 (1989).

61 Freckleton, R. P., Harvey, P. H. & Pagel, M. Phylogenetic analysis and comparative data: a test and review of evidence. *The American Naturalist* **160**, 712-726 (2002).

62 Tung Ho, L. s. & Ané, C. A linear-time algorithm for Gaussian and non-Gaussian trait evolution models. *Systematic biology* **63**, 397-408 (2014).

63 Donoghue, M. J. & Ackerly, D. D. Phylogenetic uncertainties and sensitivity analyses in comparative biology. *Phil. Trans. R. Soc. Lond. B* **351**, 1241-1249 (1996).

64 Paterno, G. B., Penone, C. & Werner, G. D. sensiPhy: An r-package for sensitivity analysis in phylogenetic comparative methods. *Methods in Ecology and Evolution* **9**, 1461-1467 (2018).

65 Adams, D. C. & Otárola-Castillo, E. geomorph: an R package for the collection and analysis of geometric morphometric shape data. *Methods in Ecology and Evolution* **4**, 393-399 (2013).

Figure legends

Fig. 1. Optimization of web anchor performance. ***(a)*** Simulated peak pull-off forces (anchor strength) vs. different dragline positions for silk properties of Tasmanian cave spiders (*H. troglodytes*) and golden orb weavers (*N. plumipes*) under vertical load. The yellow shade indicates the estimated range of c_d (for a variety of silk properties), where anchor strength is maximized. ***(b)*** Exemplary maps of interfacial stress in the silk membrane (apical view) for an orb weaver silk anchor with $c_d = 0.0$ and $c_d = 0.4$ under vertical load. Warm colours indicate high stress. Anchors reach the peak pull-off force when the interfacial stress concentration around the peeling line reaches the membrane edge. ***(c)*** Simulated anchor strength for different dragline loading angles between 15° (± parallel to substrate along spinning direction) and 165° (± parallel to substrate against spinning direction, i.e. dragline flipped over) and three different values of c_d (different colours, bold font indicates the mean c_d naturally found in this species) for silk properties of Tasmanian cave spiders. ***(d)*** Same as in (c) for silk properties of golden orb weavers. Inset shows three-dimensional displacement map and stress distribution in an anchor with $c_d = 0.4$, pulled at an angle of 75° (top-side view).

Fig. 2. Correlated evolution of web structure, behaviour and morphology. Shifts in the adaptive landscape of dragline placement c_d (left tree) and spinning choreography h_r (right tree). Branch colours denote convergent evolutionary regimes in the adaptive optimum θ as identified by *SURFACE*, with warmer colours indicating higher θs. The size of overlaid red pies indicates the posterior probability of a shift in θ in that branch, as found by *bayou*. Numbered shifts mark well supported shifts with $pp > 0.3$. White arrowheads with red outline indicate branches in which cribellum loss occurred, and green arrowheads indicate branches in which aerial web building has evolved (with a probability > 0.5). Dots at tips display c_d and h_r values measured in the extant species (grey dots represent means of individuals, black dot species means). The underlying shade indicates web building behaviour (white - no web, red - substrate web, green - aerial web) and the range of optimal anchor structure (yellow shade). Red boxes denote species with a cribellum. Schematics above symbolize anchors with a low and a high c_d (left; top view of anchor with membrane in blue and fused dragline in red) and spinning paths with a low and a high h_r (right; spinneret abducting to the right).

Fig. 3. Exceptional evolution of anchor structure in aerial web builders. ***(a)*** *AICc*-weight values for single- and two-regime evolutionary models of dragline placement c_d across 100 trees (best supporting model in bold font). A clear support for OUMAw and OUMVAw indicates that c_d evolved towards an elevated optimum and at a higher adaptive potential (and higher evolutionary rates) in aerial web builders. ***(b)*** Summary of adaptive potential α of c_d for single regime OU-models ('null'-model), and the two regimes of the best fitting OUw model across 100 trees (some extreme outliers not displayed). The black dotted line indicates an α for which the phylogenetic half-life $t½$ equals the total tree height T; below this threshold evolution becomes highly labile and BM-like (grey area). ***(c)*** Summary of the evolutionary optimum θ of c_d for single regime OU-models ('null'-model), and the two regimes of the best fitting OUw models across 100 trees. The yellow area indicates the theoretical physical optimum $c_d(F_{max})$. ***(d)*** Same as in (a) for spinning choreography h_r. A clear support for OUMAc and OUMVAc indicates that h_r evolved towards an elevated optimum and at a higher adaptive potential (and higher evolutionary rates) after cribellum loss. ***(e)*** Summary of adaptive potential α of h_r for single regime OU-models ('null'-model), and the two regimes of the best fitting OUc model across 100 trees. Same conventions as in (b). ***(f)*** Summary of the evolutionary optimum θ of h_r for single regime OU-models ('null'-model), and the two regimes of the best fitting OUc models across 100 trees. Same conventions as in (c).

Electronic Supplemental Material (*ESM*)

S1. Estimation of silk membrane stiffness.
S2. Comparing numerical model results of silk anchor efficiency with empirical data.
S3. Consensus tree.
S4. Summary of SURFACE results.
S5. Summary of bayou results.
S6. Summary of PGLS results.
S7. Summary of geometric morphometrics results.
S8. Material list and sample sizes.
S9. Terminals mapping.
S10. Genbank identifiers.
S11. R code including data and tree files (zipped archive).

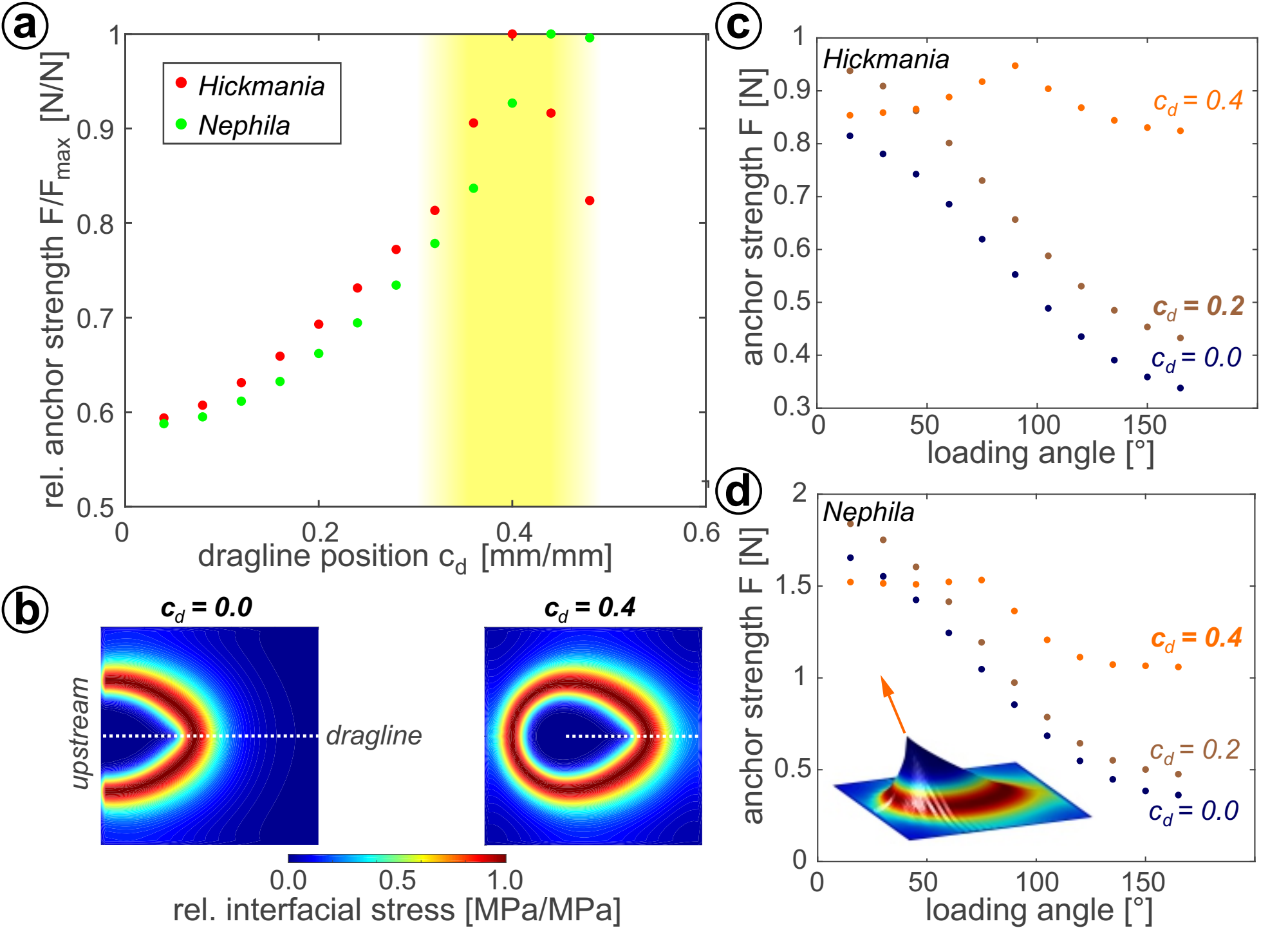
a
Hickmania
Nephila
rel. anchor strength F/F_max [N/N]
dragline position c_d [mm/mm]
b
c_d = 0.0
c_d = 0.4
upstream
dragline
0.0
0.5
1.0
rel. interfacial stress [MPa/MPa]
c
Hickmania
c_d = 0.4
c_d = 0.2
c_d = 0.0
anchor strength F [N]
loading angle [°]
d
Nephila
c_d = 0.4
c_d = 0.2
c_d = 0.0
anchor strength F [N]
loading angle [°]

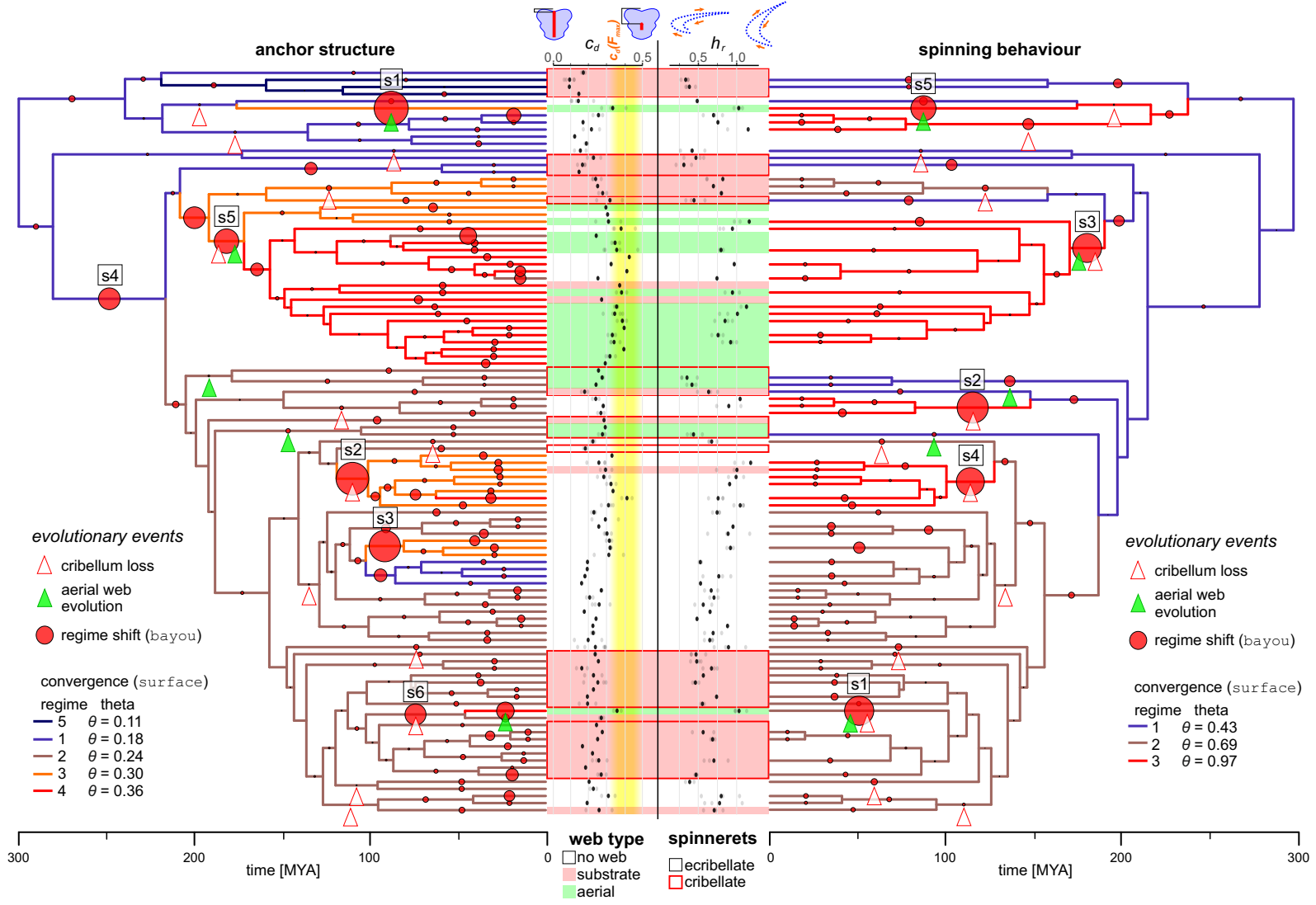
anchor structure
spinning behaviour
c_d
$c_d(F_{max})$
h_r
0.0
0.5
0.5
1.0
s1
s2
s3
s4
s5
s6
evolutionary events
cribellum loss
aerial web evolution
regime shift (bayou)
convergence (surface)
regime theta
5 θ = 0.11
1 θ = 0.18
2 θ = 0.24
3 θ = 0.30
4 θ = 0.36
1 θ = 0.43
2 θ = 0.69
3 θ = 0.97
web type
no web
substrate
aerial
spinnerets
ecribellate
cribellate
300
200
100
0
time [MYA]

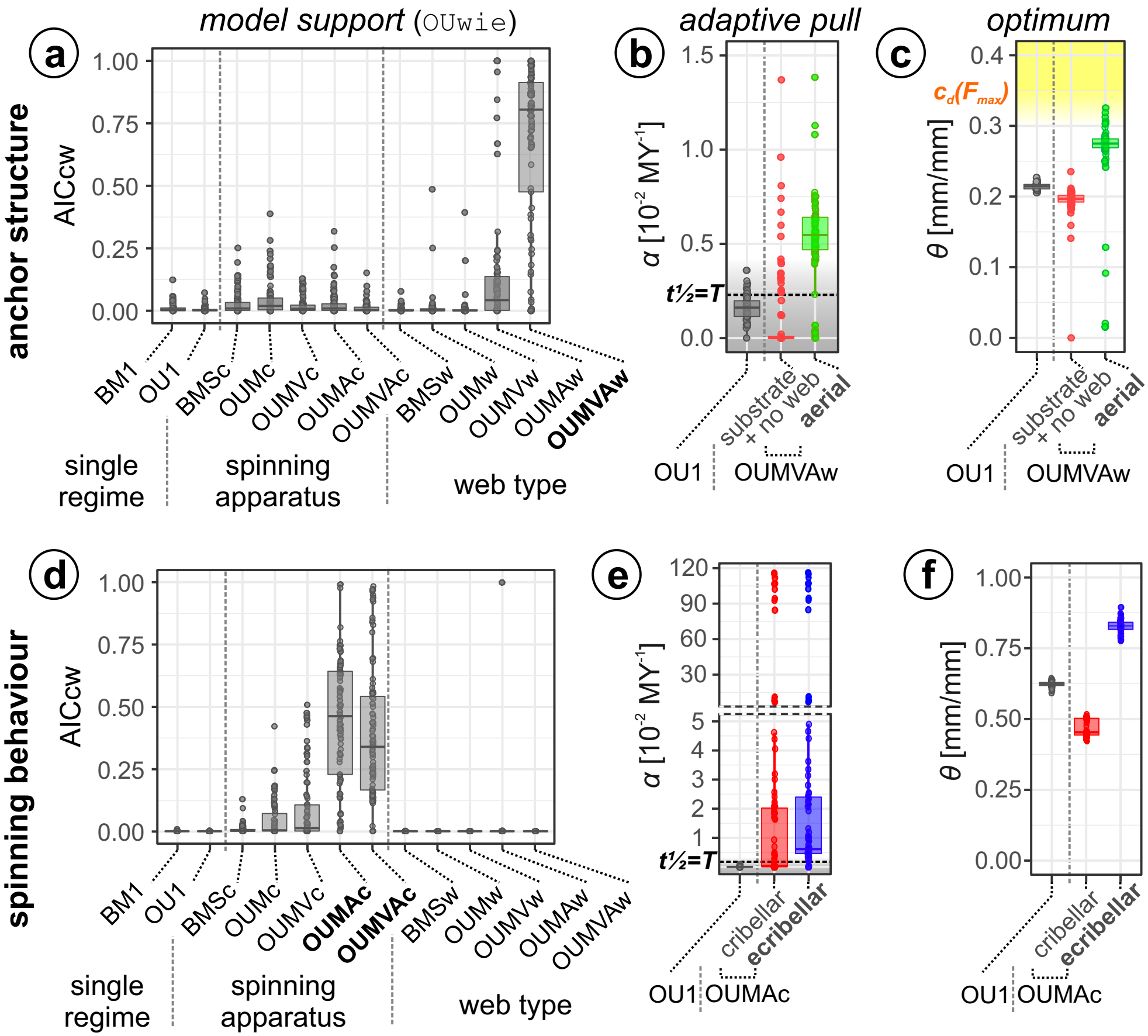
model support (OUwie)
adaptive pull
optimum
a
b
c
d
e
f
anchor structure
spinning behaviour
AICcw
α [10-2 MY-1]
θ [mm/mm]
cd(Fmax)
t½=T
BM1
OU1
BMSc
OUMc
OUMVc
OUMAc
OUMVAc
BMSw
OUMw
OUMVw
OUMAw
OUMVAw
single regime
spinning apparatus
web type
substrate + no web
aerial
cribellar
ecribellar